

Strong Roughening of Spontaneous Imbibition Fronts

Simon Gruener,¹ Zeinab Sadjadi,² Helen E. Hermes,³ Stefan U. Egelhaaf,³
Klaus Knorr,¹ Andriy V. Kityk,⁴ Heiko Rieger,² and Patrick Huber^{1,5}

¹*Experimental Physics, Saarland University, D-66041 Saarbrücken (Germany)*

²*Theoretical Physics, Saarland University, D-66041 Saarbrücken (Germany)*

³*Condensed Matter Physics Laboratory, Heinrich-Heine University, D-40225 Düsseldorf (Germany)*

⁴*Faculty of Electrical Engineering, Czestochowa University of Technology, P-42200 Czestochowa (Poland)*

⁵*Faculty of Physics and Astronomy, Pontifical Catholic University, Santiago (Chile)*

(Dated: August 14, 2011)

Imbibition is the displacement of one fluid by another immiscible fluid in a porous matrix. The dynamics and morphological evolution of the invasion front can be described by simple scaling laws. In systems with similar pore length and diameter such as paper and sand, the menisci advancement is highly correlated due to surface tension. This results in slow imbibition front roughening. Here we investigate imbibition in a sponge-like glass in which the nanopores have much longer lengths than diameters. Anomalously fast imbibition front roughening dynamics are experimentally observed by neutron imaging. Our complementary computer simulations show that this is due to the weak correlation of the menisci and occurs despite the high connectivity of the capillary network. These results reveal a new universality class of imbibition behaviour which is expected to occur in any matrix with elongated pores.

Many everyday activities involve the flow of a liquid into a porous matrix, for instance when we dunk a biscuit into coffee, clean the floor with a cloth, or get drenched with rain. The same process is also important in nature, e.g. for water to reach the tips of the tallest trees or to flow through soil, and crucial for different industrial processes, ranging from oil recovery and chromatography to food processing, agriculture, heterogeneous catalysis, and impregnation (for reviews see [1–4]).

Imbibition into a porous matrix is governed by the interplay of capillary pressure, viscous drag, volume conservation and gravity. The porous matrix often has a complex topology. Its inhomogeneities result in variations in the local bulk hydraulic permeability and in the capillary pressure at the moving interface. Nevertheless, the invasion front during solely capillarity-driven, i.e. spontaneous, imbibition advances in a simple square-root-of-time manner, according to the Lucas-Washburn law^{5,6}. This is a result of the time-independent mean capillary pressure and the increasing viscous drag in the liquid column behind the advancing front. It is valid down to nanoscopic pore sizes^{7–9} and particularly robust with regard to the geometrical complexity of the porous matrix^{1,2,10,11}. The shape of the invasion front displays universal scaling features on large length and time scales^{12–18}, which are independent of the microscopic details of the fluid and matrix. This parallels the elegance of critical phenomena.

Typically imbibition is studied using paper^{12–14} or Hele-Shaw cells^{15,16}. In these systems, pore space is laterally highly interconnected which results in a continuous liquid-gas interface and a strong lateral correlation of the advancing menisci. Similar to the surface tension of a classical liquid-gas interface¹⁹, in this situation an effective (smoothing) surface tension also exists which inhibits the interface roughening dynamics. By contrast, many real porous systems, e.g. rock and soil²⁰,

consist of pore networks with elongated pores and reduced connectivity¹. In these systems, capillarity-driven imbibition has not yet been studied due to the difficulty in following the morphological evolution of deeply buried interfaces^{21,22}.

Here we investigate the spontaneous imbibition of water into nanoporous Vycor glass (NVG), which is a silica substrate with an interconnected network of nanometer-sized, elongated pores²³ (Fig. 1). The narrow pores lead to capillary pressures of several hundred times atmospheric pressure. This means that gravity would only halt capillary rise after several kilometers and several billion years²⁴. Hence, with this system, we are able to observe pure spontaneous imbibition over unprecedented length (centimeter) and time (hours) scales. We focus on the roughening dynamics of the invasion front, which we investigate experimentally by neutron imaging and theoretically with a pore network model. Both approaches

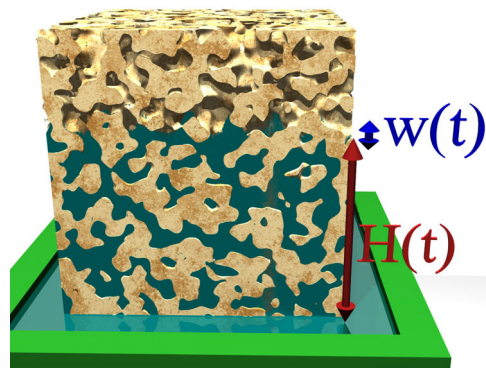


FIG. 1: **Schematic representation of spontaneous imbibition of a fluid into a porous matrix.** The arrows indicate the median rise level $H(t)$ and the invasion front width $w(t)$.

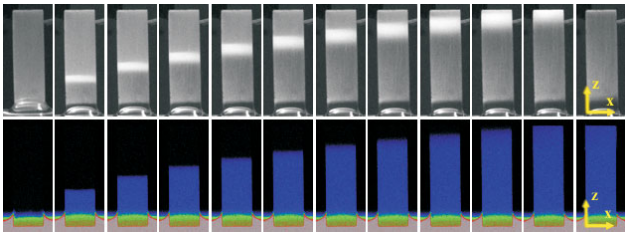


FIG. 2: **Direct observation of spontaneous imbibition of water into nanoporous Vycor glass using visible light (top row) and neutrons (lower row).** The transmitted light intensity and the local liquid concentration, i.e. the filling degree $f(x, z, t)$, are shown in grayscale and pseudocolours, respectively. Snapshots are recorded about every 15 min. The lateral direction x and the height z , i.e. the direction of capillary rise, are indicated.

show that the interface roughness as measured by the interface width $w(t)$ increases much faster than observed to date, namely $w(t) \propto t^\beta$ with $\beta \approx 0.45$. Furthermore, we find that height-height correlations of the invasion front are short-ranged and independent of time and the lateral system size. This indicates that surface tension is irrelevant for the interface roughening on macroscopic length scales.

Quantitative experimental characterization of the imbibition front

We investigate imbibition in NVG which contains pores with a mean radius $r_{av} = 4$ nm, a polydispersity of the radius of 20 %, a pore aspect ratio $5 \lesssim L/(2r_{av}) \lesssim 7$ (L being the pore length), and a porosity of about 30 %^{8,23,25,26}. (For details see Methods.) The bottom face of an empty NVG is brought into contact with the surface of a water reservoir. The Laplace pressure at the nanometer-sized menisci drives the liquid into the porous matrix.

The invasion front appears as a bright region when imaged using transmitted light (Fig. 2, top row). The pronounced light scattering is caused by filled and empty regions randomly alternating on the length scale of the wavelength of visible light²⁷. Multiple light scattering prevents a quantitative determination of the liquid distribution in the propagating front. By contrast, recent advancements in the spatial and temporal resolution of neutron imaging now allow quantitative measurements in systems such as NVG. The water distribution during capillary rise can be resolved with high precision (Fig. 2, lower row).

From the neutron images we determine the spatial and temporal evolution of the local filling degree $0 \leq f(x, z, t) \leq 1$. Due to the projection in the y -direction and the limited spatial resolution, this is the average amount of filled pore space at lateral position x , height z and time t . Its lateral average, that is the vertical concentration profile $\bar{f}(z, t) \equiv \langle f(x, z, t) \rangle_x$, is shown in

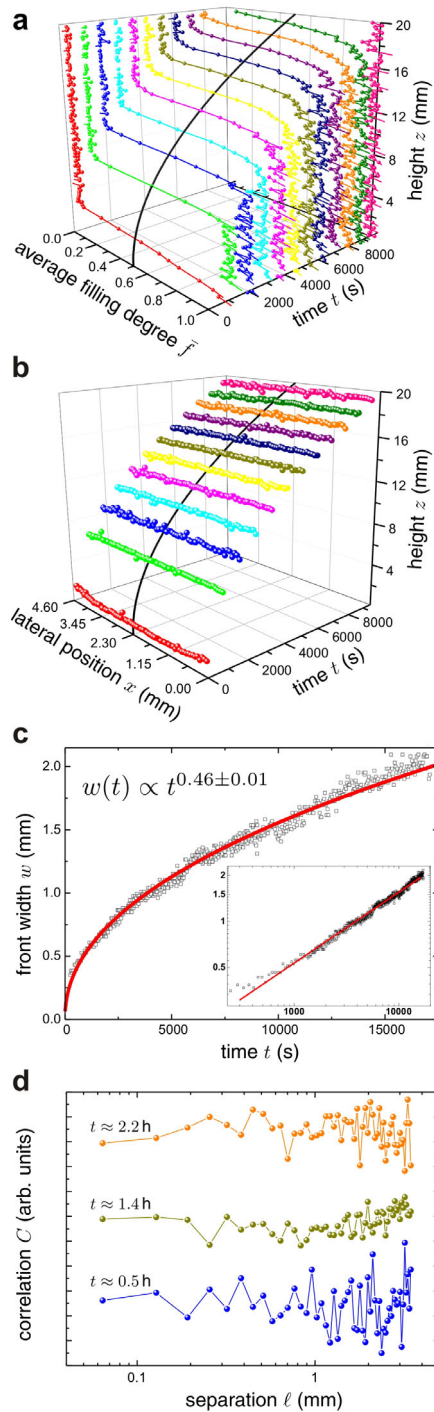


FIG. 3: **Progression and roughening of the imbibition front of water in nanoporous Vycor glass as observed by neutron imaging.** (a) Laterally-averaged filling degree $\bar{f}(z, t) \equiv \langle f(x, z, t) \rangle_x$ as a function of height z and time t . (b) Local median rise level $z(f=0.5, x, t)$ as a function of lateral position x and time t . (c) Evolution of the front width $w(t)$ along with a fit of $w \propto t^\beta$ (solid line). The inset shows the same data in a log-log representation. (d) Height-height correlation function $C(\ell, t)$ of the invasion front at three different times (as indicated). The data are shifted for clarity. In (a) and (b) the Lucas-Washburn law $z \propto \sqrt{t}$ is shown as solid line.

Fig. 3a. The time-dependence of the front height, quantified by the median rise level $H(t) \equiv \langle z(f=0.5, x, t) \rangle_x$, follows the Lucas-Washburn \sqrt{t} -law (Figs. 3a,b, solid lines), consistent with previous studies⁸. Fits of Gauss error functions yield the time-dependence of the width $w(t)$ (Fig. 3c). A fit of $w(t) \propto t^\beta$ results in a growth exponent of the width or roughness, $\beta = 0.46 \pm 0.01$ (Fig. 3c, solid line). This value significantly exceeds previous theoretical predictions, in particular those from phase-field models which are based on quenched, random fields. Such models predict slower roughening dynamics with $\beta \approx 0.19$ and a strong spatial correlation of the height fluctuations within the moving interface¹⁸.

In our experiments, we observe a projection in the y -direction, hence height fluctuations are partially averaged. Based on the local median rise level $h(x, t) \equiv z(f=0.5, x, t)$ (Fig. 3b) we calculate the height-height correlation function:

$$C(\ell, t) = \sqrt{\langle (h(x, t) - h(x+\ell, t))^2 \rangle_x}. \quad (1)$$

The observed noise in $C(\ell, t)$ (Fig. 3d) is due mainly to the limited data density and stray gamma radiation from the reactor and instrument hitting the camera. The data exhibit neither scaling of $C(\ell, t)$ with ℓ nor any indication of spatial correlations in the experimentally accessible range $60 \mu\text{m} \leq \ell \leq 4000 \mu\text{m}$. This is in contrast to all previously reported experiments and theories on imbibition front roughening.

Pore-network model

No theoretical model is available which predicts the spontaneous imbibition behaviour observed, i.e. agreement with the Lucas-Washburn law, fast roughening dynamics with a growth exponent close to $1/2$, and no detectable height-height correlation at the advancing imbibition front. (For an overview of existing models see [2].) Hence we propose a pore-network model^{28,29} adapted to our experimental situation to microscopically analyze the spontaneous imbibition dynamics in capillary networks. (For details see Methods.) Since they consist of individual, elongated capillaries, a continuous, macroscopically extended liquid-gas interface does not develop and thus correlations between menisci movements mediated by surface tension are significantly reduced.

The model consists of a two-dimensional square lattice of capillaries with laterally periodic boundary conditions. Capillaries are connected at nodes. All capillaries have the same length, while the radius of each capillary is randomly chosen from a uniform distribution with mean radius r_{av} and width $2\delta_r$, i.e. disorder strength δ_r/r_{av} .^{23,26} We present results for an aspect ratio of 2.5-10 and polydispersity $0.1 \leq \delta_r/r_{\text{av}} \leq 0.4$.

All nodes at the bottom of the lattice have zero pressure while at the menisci the Laplace pressure prevails. This pressure difference drives the flow through the capillaries. This flow is opposed by viscous drag according

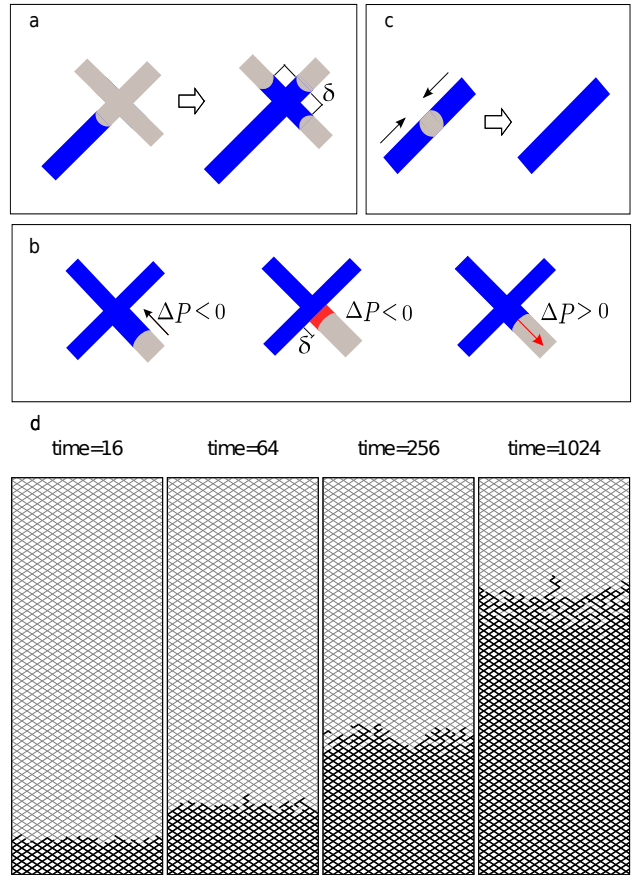


FIG. 4: **Computer simulation of spontaneous imbibition in a network of elongated capillaries.** Rules for the propagation of menisci are designed to mimic the experimental situation. (a) After reaching an empty node, the liquid immediately fills the connected capillaries for a distance δ . (b) After retracting up to δ toward a filled node, the meniscus is arrested until the pressure difference driving the liquid is again positive. (c) When two menisci meet, they merge. (d) Snapshots of configurations in a system with aspect ratio 5, polydispersity of the radius 0.3 and lattice size 16×64 at different times (as indicated in units of ns).

to Hagen-Poiseuille's law. During the whole process, volume conservation has to be maintained. The time step Δt is chosen such that each meniscus moves at most a distance $L/10$ and no meniscus crosses a node. If this would occur for one meniscus, Δt is reduced such that this meniscus reaches the next node and then 'jumps' over the node, generating new menisci in a distance $\delta = L/100$ from the node (Fig. 4a), and all other menisci are also processed with the reduced Δt . If, due to a negative pressure difference, a meniscus would retract beyond a node, the capillary is kept filled over a length δ and the meniscus arrested until the liquid advances again due to a positive pressure difference (Fig. 4b). This implementation of node crossing avoids a microscopic treatment of flow in the nodes.

Computer simulation results of imbibition

With our model, we observe a strong roughening of the imbibition front (Fig. 4d) with fast moving menisci advancing through sequences of thin capillaries and arrested menisci lagging behind. Quantitatively, the computer simulations yield a mean rise level $H(t) = \langle h_i(t) \rangle$ (where $\langle \dots \rangle$ denotes an average over all menisci labelled by the index i), which obeys the Lucas-Washburn \sqrt{t} -behaviour (Fig. 5a). The width $w(t) = (\langle h_i^2(t) \rangle - \langle h_i(t) \rangle^2)^{1/2}$ increases rapidly as $w(t) \propto t^\beta$ with $\beta = 0.42 \pm 0.01$ or 0.45 ± 0.01 for the smallest and largest polydispersity, respectively (Fig. 5b,c). We find a slight upward trend of $w(t)$ at large times (Fig. 5b, inset), which is also suggested in the experimental data (Fig. 3c) and indicates that the asymptotic value of the growth exponent might be larger. This is consistent with the fact that a smaller β is observed when the asymptotic behaviour is approached later (as in the case of the smaller polydispersity). This implies that the asymptotic value is closer to that found for the larger polydispersity with an increased uncertainty, i.e. $\beta = 0.45 \pm 0.02$. Different aspect ratios gave identical results (data not shown).

Additionally, we systematically studied finite size effects, especially on $w(t)$. Remarkably, we only find a dependence on the lateral system size N_x for the smallest system size $N_x = 4$ (Fig. 5c). This provides an upper bound for the characteristic length scale $\xi(t)$ of height-height correlations. Within the framework of the scaling theory of roughening^{30,31}, the interface width in a finite system of lateral size N_x is expected to behave as

$$w_{N_x}(t) = \langle h(x, t)^2 \rangle_x - \langle h(x, t) \rangle_x^2 \sim \begin{cases} t^\beta & \text{for } \xi(t) \ll N_x \\ \text{const.} & \text{for } \xi(t) \gg N_x \end{cases} \quad (2)$$

The data (Fig. 5c) suggest $\xi(t) < 4L$, implying that the roughening dynamics are not or are only weakly spatially correlated. This is confirmed by the height-height correlation function $C(\ell, t)$ (eq. 1, Fig. 5d), which saturates quickly (around $\ell \approx L$). Scaling theory^{30,31} predicts saturation of $C(\ell, t)$ for $\ell \gg \xi(t)$, which implies $\xi(t) = \mathcal{O}(1)$ independent of time t . This finding supports our experimental results (Fig. 3d) that any spatial roughness correlations are absent and extends its validity down to pore-pore distances and thus towards the nanometer-scale, i.e. far beyond our experimental resolution.

Experiments and simulations both yield a new roughness growth exponent

The pore-network model mimics the main feature of NVG, namely elongated pores. These inhibit the formation of a connected water-air interface and thus the inter-action of individual menisci via surface tension. Experiments and simulations exhibit corresponding behaviour, even on a quantitative level, i.e. progression of the imbibition front according to the Lucas-Washburn \sqrt{t} -law,

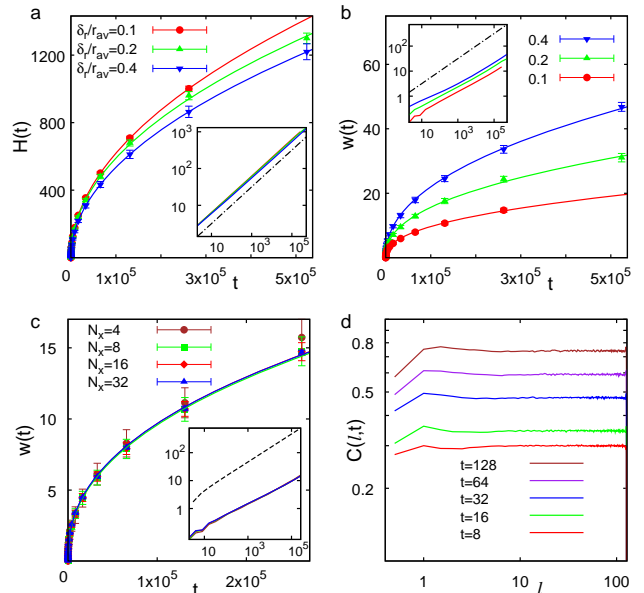


FIG. 5: Progression and roughening of the imbibition front as observed in computer simulations based on our pore-network model. Pore aspect ratio of 5 and standard lattice size $N_x \times N_z = 16 \times 1000$. Lengths are measured in units of L , times in units of ns. All data are averaged over 100 simulations with different disorder realizations, the error bars reflect the standard deviation. (a) Mean rise level $H(t) = \langle h_i(t) \rangle$ for different polydispersities δ_r/r_{av} (as indicated). The lines represent fits of $H \propto \sqrt{t}$. The inset shows the same data in a log-log representation and $H \propto \sqrt{t}$ as the dash-dotted line. (b) Evolution of the front width $w(t)$ for different polydispersities (as indicated). The lines represent fits of $w(t) \propto t^\beta$ with growth exponents $\beta = 0.42 \pm 0.01$, 0.42 ± 0.01 and 0.45 ± 0.01 for polydispersities of 0.1, 0.2 and 0.4, respectively. The inset shows the same data in a log-log representation and \sqrt{t} as the dash-dotted line. (c) Evolution of the front width $w(t)$ for a polydispersity $\delta_r/r_{av} = 0.1$ and different lateral system sizes N_x (as indicated). The line represents a fit of $w \propto t^\beta$ with $\beta = 0.42 \pm 0.01$ for $N_x > 4$. The inset shows the same data in a log-log representation, the dashed line represents an upper bound of the width, which is given by the difference between the front heights $H(t) \propto \sqrt{t}$ in two homogeneous systems with constant minimal and maximal capillary radius $r = r_{av} - \delta_r$ (slowest front propagation) and $r = r_{av} + \delta_r$ (fastest front propagation), respectively. (d) Height-height correlation $C(\ell, t)$ as a function of the distance ℓ at different times t (as indicated) for a sample with polydispersity of 0.1 and $N_x \times N_z = 128 \times 32$.

fast roughening of the front with a large growth exponent $\beta \approx 1/2$ and short range height-height correlations over a maximum of 1–2 pore lengths only. The weak lateral correlations are thus responsible for the new universality class. Furthermore they explain why our two-dimensional simulations agree with our three-dimensional experimental results. We also expect that the results are independent of the specific network, e.g. diluted honeycomb or a random graph embedded in three dimensions.

Both our experiments and simulations suggest a roughness growth exponent close to $1/2$ ($\beta \approx 0.45$). We might speculate that $1/2$ is in fact the exact asymptotic value as one would expect for a matrix of non-connected pores with random but constant radii. But non-connected pores with random variations of the radius over the pore length exhibit a lower exponent of $\beta = 1/4$ as we found using scaling arguments and checked numerically. The smaller exponent indicates an equalization of the menisci velocities in the different capillaries, which is due to the fact that in any capillary the fluid has to pass through segments of different thicknesses. Surprisingly, the introduction of connections, i.e. branch points or crossings, enhances height fluctuations and hence the front width. This is because at each branch point one meniscus can split into two (or more) upwards moving menisci with one typically moving faster than the other, or even one moving and the other stopping.

An alternative explanation for the value $\beta \approx 1/2$ has recently been proposed within the framework of a lattice gas model for spontaneous imbibition³². This is based on pure diffusion rather than a balance between capillary forces and height dependent pressure gradients. This is appropriate for silica aerogels with an extreme porosity of 87-95%, which allows for a continuous liquid-gas interface forming the invasion front. By contrast, the much smaller porosity and the characteristic capillary structure of NVG render capillary forces and height dependent pressure gradients dominant on mesoscopic length scales. It is conceivable that both descriptions asymptotically converge to a unified picture.

Pore aspect ratio determines the universality class

Our results show that spontaneous imbibition crucially depends on the pore aspect ratio. It determines the range of applicability of a capillary network model to spontaneous imbibition in porous media. For pores longer than they are wide ($L \gg r_{av}$), all menisci are well separated and do not form a continuous imbibition front. This leads to strong roughening with $\beta \approx 1/2$ as shown in our experiments and in our model. For short pores ($L \lesssim r_{av}$) neighbouring menisci coalesce, a continuous imbibition front exists and surface tension effects become important, as for imbibition in paper and sand. In this case, the capillary network model has to assume *ad hoc* an interaction between neighbouring menisci in order to include surface tension effects²⁹. An appropriate description of this situation is achieved by phase field models¹⁹, which correctly predict weak imbibition front roughening with $\beta \approx 0.19$. Thus, our work shows that the pore aspect ratio determines whether a connected air-water interface and thus surface tension-mediated interactions between individual menisci are present, which is crucial for imbibition front roughening and determines its universality class.

We want to stress that strong imbibition front roughening is not linked to the nanometer size of the pores.

However, its experimental observation over large length and time scales significantly benefits from the dominance of capillary forces over gravitational forces, which results from the nanometer-sized pores. Note that the computer simulations employ macroscopic hydrodynamic concepts only. Therefore, strong interfacial roughening is a consequence of any spontaneous imbibition process in porous structures with elongated capillaries, such as rocks and soils, independent of their macroscopic extension and mean pore diameter. Our observation of a new universality class of strong interfacial roughening is thus a very general finding, which has been made possible due to recent improvements in the resolution of neutron imaging. It is not only important to nanofluidics, but for liquid transport in porous media in general. The front roughness is crucial for many processes, such as water transport in geology, forced flux in oil recovery, glueing, dying and impregnation. Our results enable us to link the roughening dynamics during these processes to the properties of the porous materials and thus design porous materials for specific applications. It will be interesting to explore experimentally and theoretically the transition between strong and weak imbibition front roughening. This will require a detailed treatment, in particular a spatial analysis, of the menisci dynamics and the morphological evolution at pore junctions and in pore niches.

Methods

Neutron imaging. The nanoporous Vycor glass (NVG) consists of an interconnected network of elongated pores with a mean radius $r_{av} = 4$ nm, a polydispersity of the radius of 20%, a pore aspect ratio of about 5–7, and a porosity of about 30%^{8,23,25,26}. The macroscopic dimensions of the sample are $4.6 \times 4.6 \times 20$ mm³. Its faces, except the bottom face, are sealed to preclude liquid evaporation. To initiate imbibition, the bottom face of the sample is brought into contact with the surface of a water reservoir. During imbibition, the huge capillary pressure highly compresses entrapped air which is subsequently dissolved in water and hence does not affect our experiments. All experiments are performed at room temperature.

The neutron imaging experiments are performed at the ANTARES beamline of the research reactor FRM II of the Technical University München (Garching, Germany). The sample is ‘illuminated’ by a 40×40 mm² beam of cold neutrons. While silica, and thus NVG, is almost transparent to neutrons, the neutron beam is strongly attenuated by hydrogen, here water. The contrast is further enhanced by the characteristic wavelength distribution of the ANTARES beamline, which contains a large fraction of cold neutrons. The transmitted neutrons are detected using a ‘Gadox’ scintillator and a CCD camera (pixel size 15.97 μ m). The effective spatial resolution of the set-up is about 30 μ m. Series of images are recorded with an individual measurement time of 40 s and a total measurement time of up to several hours. Raw images were corrected for detection efficiency, background and noise.

Computer simulations. The pore-network model consists of capillaries arranged on a two-dimensional square lattice inclined at 45°. The system consists of N_x and N_z nodes in the horizontal and vertical directions, respectively, with

periodic boundary conditions in horizontal direction. At the nodes, four capillaries are connected to each other (Fig. 4). All capillaries have the same length L , while the radius of each capillary is chosen randomly from a uniform distribution with mean radius r_{av} and distribution width δ_r , i.e. disorder strength δ_r/r_{av} . We performed computer simulations for different lateral system sizes $4 \leq N_x \leq 32$ and a vertical size up to $N_z = 1000$, which implies a maximum height $H = \sqrt{2} N_z L$ which was not reached by the invasion front within the simulation time.

The water rises spontaneously from the bottom to the top of the lattice. The dynamics are controlled by capillary pressure, viscous drag and volume conservation. At each meniscus, i.e. for each capillary j connected to node i , we calculate the capillary pressure given by the Laplace pressure

$$P_{c,i}^j = \frac{2\sigma}{r_i^j}, \quad (3)$$

where r_i^j is the radius of the capillary and σ the surface tension ($\sigma = 72$ mN/m for water). Flow through the capillary is driven by the pressure difference $\Delta P_i^j = P_i - P_{c,i}^j$, where P_i is the pressure at node i .

According to Hagen-Poiseuille's law, the volume flux Q_i^j from node i into capillary j is

$$Q_i^j = -\frac{\pi(r_i^j)^4}{8\eta} \frac{\Delta P_i^j}{h_i^j}, \quad (4)$$

where h_i^j is the length of the liquid column in capillary j of node i and η the viscosity of the liquid ($\eta = 0.88$ mPa s for water). The volume flux Q_i^j determines the change of the liquid volume V_i^j and thus of the length of the liquid column h_i^j according to $Q_i^j = dV_i^j/dt = \pi(r_i^j)^2 dh_i^j/dt$. Hence, once the node pressures P_i are known, the time dependencies of the heights $h_i^j(t)$ are given by ordinary differential equations.

The node pressures P_i are determined by the boundary conditions and volume conservation. The boundary conditions are the Laplace pressure at the menisci, $P_{c,i}^j$, and zero pressure at all nodes at the bottom of the lattice which are

connected to the water reservoir. The volume conservation at each node is given by

$$\sum_j Q_i^j = 0, \quad (5)$$

which corresponds to Kirchhoff's law. The sum runs over all capillaries j attached to node i . The resulting set of sparse linear equations is numerically solved to obtain the node pressures P_i for a given meniscus height configuration h_i^j . The differential equations for h_i^j are then numerically integrated using an implicit Euler scheme for time-stepping. Note that, due to the nanometer-sized capillaries, capillary pressure dominates gravity, which can thus be neglected.

The time step Δt is chosen such that each meniscus moves at most a distance $L/10$ and that no meniscus crosses a node. If this would occur the move is rejected and the time step Δt reduced to the time interval within which this meniscus reaches the next node. Then the liquid is immediately moved a distance $\delta = L/100$ into the adjacent capillaries (Fig. 4a). All other menisci are processed with the reduced Δt . Similarly, if the meniscus retracts due to a negative pressure difference, $\Delta P_i^j < 0$, the meniscus is arrested when it has approached the node up to a distance δ . Thus a liquid column with a length of at least δ is kept in the capillary, i.e. $h_i^j \geq \delta$ always holds. The meniscus is released when $\Delta P_i^j > 0$ (Fig. 4b). When two menisci meet, they merge and the capillary thus is completely filled (Fig. 4c), which mimics the absence of entrapped air in our experimental system.

During a computer simulation of the time evolution of the model, the average rise level $H(t) = \langle h_i(t) \rangle$ of the invading front and its width $w(t) = (\langle h_i^2(t) \rangle - \langle h_i(t) \rangle^2)^{1/2}$ are calculated at different times t . Since the invasion front contains overhangs and voids, the average $\langle \dots \rangle$ is taken over all menisci indexed by i . The presented data are averaged over 100 simulation runs using different disorder realizations. The statistical error of this average represents the error bars of the simulation results.

-
- [1] Sahimi M. Flow phenomena in rocks — from continuum models to fractals, percolation, cellular-automata, and simulated annealing. *Rev. Mod. Phys.* **65**, 1393 (1993).
- [2] Alava M, Dubé M, and Rost M. Imbibition in disordered media. *Adv. Phys.* **53**, 83 (2004).
- [3] Halpinhealy T and Zhang YC. Kinetic roughening phenomena, stochastic growth directed polymers and all that. *Phys. Rep.* **254**, 215 (1995).
- [4] Hinrichsen H. Non-equilibrium critical phenomena and phase transitions into absorbing states. *Adv. Phys.* **49**, 815 (2000).
- [5] Lucas R. Über das Zeitgesetz des kapillaren Aufstiegs von Flüssigkeiten. *Kolloid Zeitschrift* **23**, 15 (1918).
- [6] Washburn EW. The dynamics of capillary flow. *Phys. Rev.* **17**, 273 (1921).
- [7] Dimitrov DI, Milchev A, and Binder K. Capillary rise in nanopores: Molecular dynamics evidence for the Lucas-Washburn equation *Phys. Rev. Lett.* **99**, 054501 (2007).
- [8] Gruener S, Hofmann T, Wallacher D, Kityk AV, and Huber P. Capillary rise of water in hydrophilic nanopores. *Phys. Rev. E* **79**, 067301 (2009).
- [9] Gruener S and Huber P. Spontaneous imbibition dynamics of an n-alkane in nanopores: Evidence of meniscus freezing and monolayer sticking. *Phys. Rev. Lett.* **103**, 174501 (2009).
- [10] Courbin L, Denieul E, Dressaire E, Roper M, Ajdari A, Stone HA. Imbibition by polygonal spreading on microdecorated surfaces. *Nature Materials* **6**, 661 (2007).
- [11] Reyssat M, Courbin L, Reyssat E, Stone HA. Imbibition in geometries with axial variations. *J. Fluid Mech.* **615**, 335 (2008).
- [12] Buldyrev SV, Barabási AL, Caserta F, Havlin S, Stanley HE, and Vicsek T. Anomalous interface roughening in porous media — experiment and model. *Phys. Rev. A* **45**, R8313 (1992).
- [13] Horváth VK and Stanley HE. Temporal scaling of interfaces propagating in porous media. *Phys. Rev. E* **52**, 5166 (1995).
- [14] Miranda AM, Menezes-Sobrinho IL, and Couto MS. Sponta-

- neous imbibition in newspaper sheets. *Phys. Rev. Lett.* **104**, 086101 (2010).
- [15] Hernández-Machado A *et al.* Interface roughening in Hele-Shaw flows with quenched disorder: Experimental and theoretical results. *Europhys. Lett.* **55**, 194 (2001).
- [16] Geromichalos D, Mugele F, and Herminghaus S. Nonlocal dynamics of spontaneous imbibition fronts. *Phys. Rev. Lett.* **89**, 104503 (2002).
- [17] Planet R, Pradas M, Hernández-Machado, and J. Ortin. Pressure-dependent scaling scenarios in experiments of spontaneous imbibition. *Phys. Rev. E* **76**, 056312 (2007).
- [18] Dubé M, Daneault C, Vuorinen V, Alava M, and Rost M. Front roughening in three-dimensional imbibition. *Eur. Phys. J. B* **56**, 15 (2007).
- [19] Dubé M, Rost M, and Alava M. Conserved dynamics and interface roughening in spontaneous imbibition: A critical overview. *Eur. Phys. J. B* **15**, 691 (2000).
- [20] Song YQ, Ryu S, and Sen PN. Determining multiple length scales in rocks. *Nature* **406**, 178 (2000).
- [21] Callaghan PT *et al.* Diffraction-like effects in NMR diffusion studies of fluids in porous solids. *Nature* **351**, 467 (1991).
- [22] Howle L, Behringer RP, Georgiadis J. Visualization of convective fluid-flow in a porous-medium. *Nature* **362**, 230 (1993).
- [23] Gelb LD and Gubbins KE. Characterization of porous glasses: Simulation models, adsorption isotherms, and the Brunauer-Emmett-Teller analysis method. *Langmuir* **14**, 2097 (1998).
- [24] Caupin F, Cole MW, Balibar S, and Treiner J. Absolute limit for the capillary rise of a fluid. *Europhys. Lett.* **82**, 56004 (2008).
- [25] Gruener S. *Rheology and Dynamics of Simple and Complex Liquids in Mesoporous Matrices*. Ph.D. thesis, Saarland University, Saarbrücken, Germany (2010).
- [26] Levitz P, Ehret G, Sinha SK, and Drake JM. Porous Vycor glass: The microstructure as probed by electron microscopy, direct energy transfer, small-angle scattering, and molecular adsorption. *J. Chem. Phys.* **95**, 6151 (1991).
- [27] Page JH, Liu J, Abeles B, Deckman HW, and Weitz DA. Pore-space correlations in capillary condensation in Vycor. *Phys. Rev. Lett.* **71**, 1216 (1993).
- [28] Aker E, Måløy KJ, Hansen A, and Batrouni GG. A two-dimensional network simulator for two-phase flow in porous media. *Transp. Porous Med.* **32**, 163 (1998).
- [29] Lam CH and Horváth VK. Pipe network model for scaling of dynamic interfaces in porous media. *Phys. Rev. Lett.* **85**, 1238 (2000).
- [30] Barabási AL and Stanley HE. *Fractal Concepts in Surface Growth* (Cambridge University Press, New York, 1995).
- [31] Krug J. Origins of scale invariance in growth processes. *Adv. Phys.* **46**, 139 (1997).
- [32] Leoni F, Kierlik E, Rosinberg ML, and Tarjus G. Spontaneous imbibition in disordered porous solids: A theoretical study of helium in silica aerogels. *Langmuir* **27**, 8160 (2011).

Acknowledgments

We acknowledge FRM II for providing beam time. We are grateful to our local contacts Michael Schulz, Elbio Calzada and Burkhard Schillinger. We thank Mikko Alava for helpful discussions. Part of this work was supported by the DFG priority program 1164, Nano- & Microfluidics (Grant. No. Hu 850/2) and the DFG graduate school 1276, 'Structure formation and transport in complex systems' (Saarbrücken).

Author Contributions

S.G. and H.H. carried out the neutron radiography experiments, Z.S. performed the computer simulations for the pore network model. S.G., H.H., S.E., K.K., A.V.K. and P.H. designed, discussed and analyzed the experiments, Z.S. and H.R. designed and analyzed the theoretical model. All authors contributed to the writing of the manuscript.

Competing Financial Interests statement

The authors declare no competing financial interests.